


## Article

# Spatiotemporal Variation of Vegetation Productivity and Its Feedback to Climate Change in Northeast China over the Last 30 Years

Ling Hu <sup>1,2</sup>, Wenjie Fan <sup>1,2,\*</sup> , Wenping Yuan <sup>3</sup>, Huazhong Ren <sup>1,2</sup>  and Yaokui Cui <sup>1,2</sup>

<sup>1</sup> Institute of Remote Sensing and Geographic Information System, School of Earth and Space Sciences, Peking University, Beijing 100871, China; hul@pku.edu.cn (L.H.); renhuazhong@pku.edu.cn (H.R.); yaokuicui@pku.edu.cn (Y.C.)

<sup>2</sup> Beijing Key Lab of Spatial Information Integration and 3S Application, Peking University, Beijing 100871, China

<sup>3</sup> School of Atmospheric Sciences, Sun Yat-Sen University, Guangzhou 519082, China; yuanwp3@mail.sysu.edu.cn

\* Correspondence: fanwj@pku.edu.cn; Tel.: +86-010-6275-5085

**Abstract:** Gross primary productivity (GPP) represents total vegetation productivity and is crucial in regional or global carbon balance. The Northeast China (NEC), abundant in vegetation resources, has a relatively large vegetation productivity; however, under obvious climate change (especially warming), whether and how will the vegetation productivity and ecosystem function of this region changed in a long time period needs to be revealed. With the help of GPP products provided by the Global LAnd Surface Satellite (GLASS) program, this paper gives an overview of the regional feedback of vegetation productivity to the changing climate (including temperature, precipitation, and solar radiation) across the NEC from 1982 to 2015. Analyzing results show a slight positive response of vegetation productivities to warming across the NEC with an overall increasing trend of GPP<sub>GS</sub> (accumulated GPP within the growing season of each year) at 4.95 g C/m<sup>2</sup> · yr<sup>−2</sup> over the last three decades. More specifically, the growth of crops, rather than forests, contributes more to the total increasing productivity, which is mainly induced by the agricultural technological progress as well as warming. As for GPP in forested area in the NEC, the slight increment of GPP<sub>GS</sub> in northern, high-latitude forested region of the NEC was caused by warming, while non-significant variation of GPP<sub>GS</sub> was found in southern, low-latitude forested region. In addition, an obvious greening trend, as reported in other regions, was also found in the NEC, but GPP<sub>GS</sub> of forests in southern NEC did not have significant variations, which indicated that vegetation productivity is not bound to increase simultaneously with greening, except for these high-latitude forested areas in the NEC. The regional feedback of vegetation productivity to climate change in the NEC can be an indicator for vegetations growing in higher latitudes in the future under continued climate change.

**Keywords:** vegetation productivity; Northeast China; climate change; spatiotemporal distribution



**Citation:** Hu, L.; Fan, W.; Yuan, W.; Ren, H.; Cui, Y. Spatiotemporal Variation of Vegetation Productivity and Its Feedback to Climate Change in Northeast China over the Last 30 Years. *Remote Sens.* **2021**, *13*, 951. <https://doi.org/10.3390/rs13050951>

Academic Editor: Kenji Omasa

Received: 20 January 2021

Accepted: 1 March 2021

Published: 3 March 2021

**Publisher's Note:** MDPI stays neutral with regard to jurisdictional claims in published maps and institutional affiliations.



**Copyright:** © 2021 by the authors. Licensee MDPI, Basel, Switzerland. This article is an open access article distributed under the terms and conditions of the Creative Commons Attribution (CC BY) license (<https://creativecommons.org/licenses/by/4.0/>).

## 1. Introduction

Gross Primary Productivity (GPP) of a terrestrial ecosystem refers to the amounts of organic compounds accumulated by green vegetations through assimilating carbon dioxide from the atmosphere via photosynthesis and a series of internal physiological processes [1–3]. GPP can partially offset anthropogenic CO<sub>2</sub> emissions [3–6], so that vegetation plays a critical role in the global carbon balance. Statically, vegetation can store about 500 Gt of carbon, which accounts for 20% of all carbon in the terrestrial biosphere [7].

To date, studies [8,9], using leaf area index (LAI) as a reference, found a significant global vegetation greening; however, the question of whether the vegetation productivity and ecosystem function varies under the obvious vegetation greening has yet to be unraveled. Compared with widely discussed leaf area (LAI or some vegetation indexes)

variation, the variation of vegetation productivity is of more practical significance, because it can not only illustrate the variation of vegetation growth but also reflect vegetation's feedback to the carbon cycle. Satellite-based vegetation productivity inversion generally employ Production Efficiency Models (PEMs), which are based on the Monteith's light use efficiency (LUE) theory [10,11]. There are a lot of different GPP products for a great amount of satellite datasets existing nowadays, e.g., using the SEVIRI/MSG satellite products to derive daily GPP [12]. Till now, the Moderate Resolution Imaging Spectroradiometer (MODIS) GPP product (MOD17) [13] is widely used [14,15]; however, the MOD17 can only provide GPP products since 2000, which is not long enough for analyzing the spatiotemporal interaction between vegetation and ecosystem. The Global LAnd Surface Satellite (GLASS) program provides GPP product covering with the longest time period (1982–2015), and it has been verified at 54 eddy covariance sites covering six major terrestrial biomes: deciduous broadleaf forests, mixed forests, evergreen needleleaf forests, grasslands, savannas, and croplands [16,17], providing a reliable and useful data source for the evaluation of terrestrial ecosystems carbon storage capacity.

The Northeast China (NEC) is a crucial zone in regional, even global carbon balance because there are abundant vegetation resources: there distributes one-third of forests in China, with boreal forests distributing in the north and southeast NEC, moreover, the boreal forests in the NEC are characterized with high carbon density, high carbon storage, and slow decomposition [18] and are revealed as an important carbon sink in China with 3.44–4.63 Pg carbon storage [19]. Additionally, the NEC is one of the most important agricultural bases in China, providing about one-third of the national grain over the last three decades [20]. What's more, as a transition region from middle to high latitude as well as one of the most climate-sensitive areas in China, the average air temperature in the NEC has increased by 0.38 °C per decade over the past five decades [21], increasing more significantly since the 1980s [22]. This kind of warming has greatly changed vegetation growth in national or global scale due to response of plant respiration, photosynthesis, and evapotranspiration to climate change [23–26]. For instance, Zhu et al. [8] found that rising temperatures have resulted in greening of the high latitudes and the Tibetan Plateau, while Yuan et al. [27] revealed a turning point in late 1990s of global vegetation productivity from increasing to decreasing due to a sharp increase in VPD (Vapor Pressure Deficit). All in all, under the circumstance of obvious climate change, the NEC is a representative place for analyzing regional feedback of vegetation productivity to global warming.

A majority of studies focusing on vegetation dynamics in the NEC use LAI or vegetation index (e.g., NDVI) as indicators [28–33]. A few studies [34–37] focused on the spatiotemporal variation of net primary productivity (NPP) over a short time period. For example, using a statistic-based multiple regression model, Ji et al. [37] simulated forest NPP across China and then revealed a significant increasing of forest NPP in Northeast China from 2000 to 2018. However, seldom have studies focused on analyzing vegetation productivity under climate change across the entire NEC over a relatively long period of time, and thus, it is necessary to have a thorough analysis on the spatiotemporal variation of vegetation productivities in the NEC, which can provide an example of interactions between vegetation and climate in other higher latitude place in the future.

In this article, our aims can be summarized as three parts: (1) detect the spatiotemporal trends of vegetation productivity across the NEC from 1982 to 2015, (2) quantify the contribution of three meteorological factors (daily average temperature, precipitation, and daily solar radiation) on vegetation productivity, and (3) compare the relationship between GPP and commonly used LAI.

## 2. Materials and Methods

### 2.1. Study Area

The NEC consists administratively of three provinces in China: Liaoning, Jilin, and Heilongjiang provinces (Figure 1a). It has a total area of 787,300 km<sup>2</sup> and had a population of about 108 million in 2019. The region is separated from Far Eastern Russia to the north

primarily by the Amur, Argun, and Ussuri Rivers, from North Korea to the south by the Yalu and Tumen Rivers, and from the Inner Mongolian Autonomous Region to the west by the Greater Khingan Range.

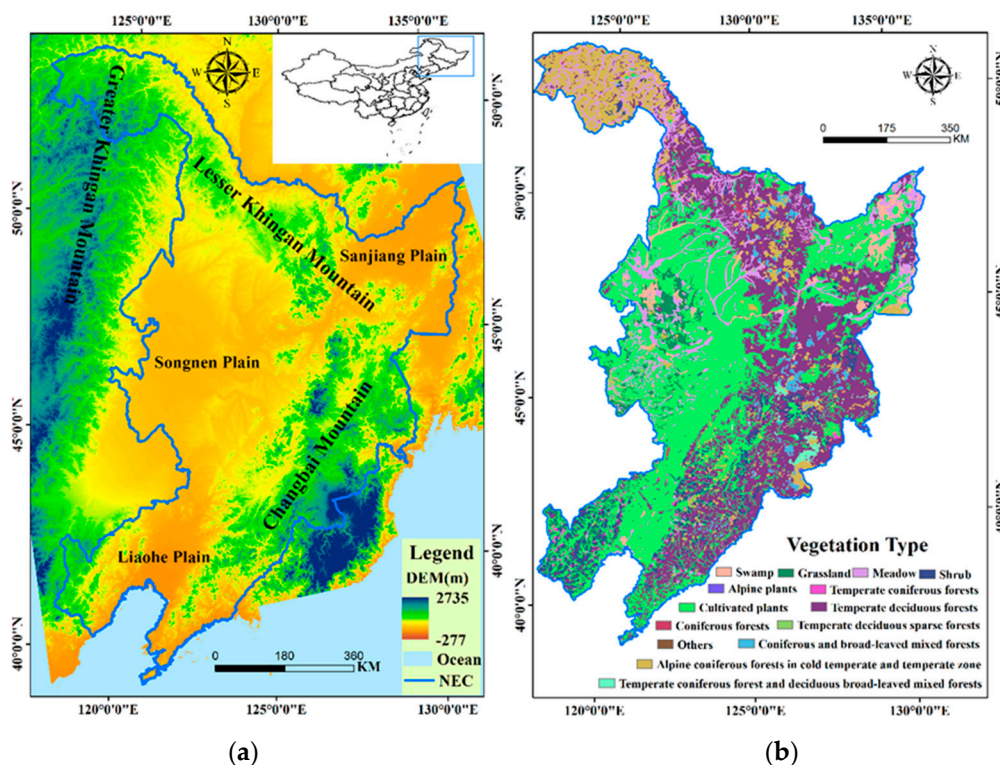


**Figure 1.** (a) Location of the study area with elevation from a Digital Elevation Model (DEM) and (b) Vegetation types of the Northeast China (NEC). (Vegetation type is provided by the Moderate Resolution Imaging Spectroradiometer (MODIS) MCD12Q1 datasets [38] in 2015).

Across from mid to high latitude (approximately 39–53° N), the NEC has a large variation in annual average temperature from 10 °C in south to −5.5 °C in north. Moreover, located at the northernmost region of China, the NEC contains the coolest region in China.

The accumulated temperature greater than 0 °C is around 2000–4200 °C, and the average temperature during summer is 20–25 °C. Influenced by the Eastern Monsoon of China, the NEC has a great variation in annual precipitation, decreasing from wet southeast (900 mm) to semi-arid northwest (400 mm), and a majority of precipitation occurs in summer (July to September).

There are three mountains: the Greater Khingan Mountain (GKM), the Lesser Khingan Mountain (LKM), and the ChangBai Mountain (CBM) (Figure 1a) that form important natural barriers for the NEC, so that the NEC can be divided into four zones (one plain and three mountains). The heartland of the NEC is the Northeast China Plain (Figure 1a, including Sanjiang Plain, Songnen Plain, and Liaohe Plain), which mainly located at the western NEC and grows a lot of crops (Figure 1b) for its rich, deep, black soil. Owning these plains, the NEC is one of the most important centers of commercial agriculture in China for both food grains (wheat, rice, and maize) and economic crops (soybean and sugar beets). The rest three mountainous zones also play a crucial role in ecosystem function. There are a great amount of forests growing in these three mountains, e.g., the LKM and the CBM are widely covered with broadleaved deciduous forests, and the GKM owns the special bright coniferous forest which is the southern boundary of the Boreal forests of Eurasia.

## 2.2. Data

### 2.2.1. GPP Datasets

GPP data used in this paper were provided by the GLASS program [39]. Generally, the GPP can be estimated using the LUE model as follows:

$$GPP = PAR \times fPAR \times \varepsilon_{\max} \times f, \quad (1)$$

where  $PAR$  is the incident photosynthetically active radiation ( $\text{MJ m}^{-2}$ ) per time period (e.g., day or month),  $fPAR$  is the fraction of  $PAR$  absorbed by the vegetation canopy,  $\varepsilon_{\max}$  is the potential LUE ( $\text{g C m}^{-2} \text{MJ}^{-1} \text{APAR}$ ) without environment stress, and  $f$  is a scalar varying from 0 to 1 and represents the effects of temperature, moisture, and other environmental conditions on LUE.

GLASS-GPP products were estimated using an improved EC-LUE (Eddy Covariance Light Use Efficiency) model, which is derived by satellite data and eddy covariance measurements [16,17]. There are four kinds of input parameters: NDVI,  $PAR$  (photosynthetically active radiation), air temperature, and the Bowen ratio of sensible-to-latent heat flux. NDVI datasets are provided by Advanced Very High Resolution Radiometer (AVHRR), which cover a long period starting from 1979. Net radiation ( $R_n$ ), air temperature ( $T$ ), relative humidity ( $R_h$ ), and photosynthetically active radiation ( $PAR$ ) from the MERRA (Modern Era Retrospective-Analysis for Research and Applications) archive [40] were used in GPP retrieval. The MERRA dataset was provided by the NASA. Its theory uses a fixed global atmospheric model and data assimilation system to analyze the historical satellite and conventional data records into a continuous global gridded dataset. The spatial resolution was  $0.5^\circ$  latitude by  $0.6^\circ$  longitude.

The GLASS-GPP datasets provides datasets covering from 1982 to 2015 with a spatial resolution of  $0.05^\circ$  and a temporal resolution of 8 days. We downloaded 1564 scenes with 46 scenes per year, and then used the Savitzky-Golay [41] filter to correct errors and fill gaps. After a series of re-projection, extraction, we acquired the available time series of GPP of the NEC. Aiming to analyzing inter-annual variation of GPP, we calculated accumulated GPP during the growing season (April to October) of each year (denoted as  $GPP_{GS}$ , hereafter) and, finally, acquired the 34-year  $GPP_{GS}$  time series for further analysis.

### 2.2.2. Auxiliary Datasets

For the attribution analysis of the spatiotemporal GPP variation, there are two kinds of datasets: the meteorological datasets and human intervention indices.

The meteorological datasets used in this study came from the China Meteorological Forcing Datasets [42], which can be acquired from the Cold and Arid Regions Science Data Center [43]. Specifically, the air temperature dataset was produced by merging observations from 740 meteorological stations of China Meteorological Administration (CMA) into the corresponding Global Land Data Assimilation System version 1 (GLDAS-1) dataset [44]. The precipitation dataset was produced by combining the observations from the 740 CMA stations, the Tropical Rainfall Measuring Mission (TRMM) 3B42 precipitation products [45], and the GLDAS-1 rainfall rate data. The downward solar radiation was constructed by correcting the Global Energy and Water Cycle Experiment-Surface Radiation Budget shortwave radiation dataset [46] with radiation estimates from meteorological station observations.

We downloaded reanalyzed meteorological data (including daily average temperature, daily precipitation rate, and daily solar radiation) with monthly temporal resolution and spatial resolution of  $0.1^\circ \times 0.1^\circ$ . First, daily average temperature and daily radiation data are averaged within the growing season of each year, and the daily precipitation rate were translated into accumulated precipitation within the growing season of each year to obtain yearly accumulated precipitation from 1982 to 2015. In the next step, the meteorological datasets were downscaled to  $0.05^\circ$  to match the spatial resolution of GPP datasets for correlation analysis. Finally, time series of yearly average temperature, yearly accumulated



precipitation, and yearly average radiation within the growing season from 1982 to 2015 were acquired for further analysis.

Human intervention indices are also considered in this study since crops are heavily influenced by human activities, so the assessment of the impacts of human intervention on crops is necessary. This study considered three indices, which can quantify the impacts of human interventions, i.e., Cropland Area (CA), Crop Yield per Area (CYA), and Irrigated Area (IA). All these indices were provided by the National Agriculture Database (Statistics Bureau of China) [47]. The detailed impacts of human intervention on GPP are shown in Section 4.1 as an additional analysis.

### 2.3. Statistical Analysis

#### 2.3.1. Mann-Kendall Trend Test

The Mann-Kendall (MK) test is a rank-based non-parametric test for detecting a monotonic trend in a time series. The method was originally used by Mann (1945) [48], and the test-statistic distribution was subsequently derived by Kendall (1975) [49]. It is frequently used for trend detection in hydrologic research [50]. In this study, we use the MK test to detect monotonic trends in the GPP data series as the test is more powerful than ordinary parametric trend tests for non-normally distributed series [51].

The MK test statistics ( $S$ ) for a series  $x_1, x_2, \dots, x_n$  can be given by

$$\text{sign}(x_j - x_i) = \begin{cases} 1; & \text{if } x_j > x_i \\ 0; & \text{if } x_j = x_i \\ -1; & \text{if } x_j < x_i \end{cases}, \quad (2)$$

$$S = \sum_{i=1}^{N-1} \sum_{j=i+1}^N \text{sign}(x_j - x_i) \quad (3)$$

where  $N$  is the length of the dataset and  $x_i$  and  $x_j$  denote the data values at times  $i$  and  $j$ . A negative value of  $S$  indicates a decreasing trend, while a positive value indicates an increasing trend [52]. Statistical significance of the trend is checked using the variance of the MK statistics, while  $N > 10$ , which is calculated as

$$\text{Var}(s) = \frac{n(n-1)(2n+5) - \sum_{i=1}^P t_i(t_i-1)(2t_i+5)}{18}, \quad (4)$$

where  $P$  is the number of tied groups, the summary sign ( $\Sigma$ ) denotes the summation over all tied groups, and  $t_i$  is the number of data in the  $i$ th (tied) group. If the tied groups are not available, this summation process is excluded from the equation.

The standard  $Z$  value of the test statistics can be estimated by the following formula.

$$Z = \begin{cases} \frac{S-1}{\sqrt{\text{Var}(S)}}; & \text{if } S > 0 \\ 0; & \text{if } S = 0 \\ \frac{S+1}{\sqrt{\text{Var}(S)}}; & \text{if } S < 0 \end{cases}. \quad (5)$$

If the computed standard  $Z$  value is greater than the critical value of the standard normal distribution at the specified significance level ( $\alpha$ ), it is considered to be significant trend, and the null hypothesis is rejected.

#### 2.3.2. Pearson Correlation

Pearson correlation is a standard parametric method used to analyze the relationship between two variables. It can be expressed as follows.

$$r = \frac{\sum_{i=1}^n (x_i - \bar{x})(y_i - \bar{y})}{\sqrt{\sum_{i=1}^n (x_i - \bar{x})^2} \sqrt{\sum_{i=1}^n (y_i - \bar{y})^2}}, \quad (6)$$

where  $x_i$  and  $y_i$  ( $i = 1, 2, \dots, n$ ) are time series for two variables,  $\bar{x}$  and  $\bar{y}$  are multi-year average values of two variables, and  $r$  is the correlation coefficient. A value of  $r > 0$  indicates a positive correlation between two variables, whereas  $r < 0$  suggests a negative correlation. The absolute value of  $r$  can represent the closeness of two variables, i.e., the larger the value of  $r$ , the closer the two variables are and vice versa. All the correlation coefficients were conducted using the 0.05 significance level.

### 2.3.3. Standardized Multivariate Linear Regression Model

Unlike the Pearson correlation method, the Standardized Multivariate Linear Regression (SMLR) method uses Gaussian normalized values in place of the original ones. Thus, the effects of changes in different factors can be compared. The SMLR model separates the relative contribution of each factor. The coefficient before each variable represents its importance in partitioning the SMLR model, and the fitting coefficients (R) of SMLR represent the combined effects of driven factors to GPP. The SMLR model is expressed as follows:

$$\frac{GPP - \overline{GPP}}{\sigma_{GPP}} = \beta_0 + \beta_1 \frac{ED_1 - \overline{ED_1}}{\sigma_1} + \dots + \beta_n \frac{ED_n - \overline{ED_n}}{\sigma_n}, \quad (7)$$

where  $ED_i$  ( $i = 1, 2, \dots, n$ ) are influencing factors;  $\overline{GPP}$  and  $\overline{ED_1}$  are multi-year mean values of  $GPP_{GS}$  and influencing factors, respectively;  $\sigma_{GPP}$  and  $\sigma_{ED}$  are standard deviations of  $GPP_{GS}$  and influencing factors, respectively, during the study period; and  $\beta_1, \beta_2, \dots, \beta_n$  are regression coefficients that represent the importance to  $GPP_{GS}$ . Factors with a larger coefficient are assumed to contribute more to the variation in  $GPP_{GS}$ , and the one with largest coefficient was identified as the dominant factor to  $GPP_{GS}$  in our study area during 1982–2015.

Before using the SMLR model, the Variance Inflation Factor (VIF) is calculated to examine multicollinearity among the influencing factors. The F-test is conducted on the model, while the  $t$ -test is conducted on the coefficients before each influencing factor. Significant tests were those below the 0.05 significance level.

## 3. Results

### 3.1. Spatiotemporal Distribution and Variation of GPP

Figure 2a reveals an obvious increasing trend of multi-year average  $GPP_{GS}$  from north to south and from west to east in the NEC, which is consistent with the spatial distribution of vegetation types and climate. The productivity of forests ranges from 700 to 1500 g C/m<sup>2</sup>. yr<sup>−1</sup>, which is obviously larger than that of crops (50–700 g C/m<sup>2</sup>. yr<sup>−1</sup>), and the productivity of forests in warm-humid lower latitude regions is about 1000–1500 g C/m<sup>2</sup>. yr<sup>−1</sup>, larger than that of forests in cold-dry regions (700–1000 g C/m<sup>2</sup>. yr<sup>−1</sup>).

Spatial distribution of inter-annual variation of  $GPP_{GS}$  in the NEC is shown in Figure 2b which owns an overall increasing trend, though great spatial heterogeneity exists. Specifically, the western NEC growing with crops has the largest  $GPP_{GS}$  increment (over 11 g C/m<sup>2</sup>. yr<sup>−2</sup>), followed by a slight increment of  $GPP_{GS}$  in the GKM and LKM (around 3–7 g C/m<sup>2</sup>. yr<sup>−2</sup>) covered with forests, while the variation of  $GPP_{GS}$  is not significant for the majority regions of CBM with sporadic pixels showing increases. Statistically, around 66.4% of the regions in the NEC has an increasing trend in  $GPP_{GS}$ , among which the area of croplands accounts for 67.3%.

We further identified the inter-annual variation of zonal  $GPP_{GS}$  at five regions: the whole NEC, plain, GKM, LKM, and CBM. There is an overall increasing trend of the whole NEC (the change ratio (denoted as CR, hereafter) = 4.95 g C/m<sup>2</sup>. yr<sup>−2</sup>;  $p < 0.01$ ) from 1982 to 2015 as shown in Figure 3a, which is mostly attributed to the growth of crops in the plain (Figure 3b). Crops growing in the NEC have a stable increase with the largest amplitude (CR = 7.47 g C/m<sup>2</sup>. yr<sup>−2</sup>;  $p < 0.01$ ), while, in the other three forested regions,  $GPP_{GS}$  shows a much smaller increasing trend (LKM: CR = 5.35 g C/m<sup>2</sup>. yr<sup>−2</sup>,  $p < 0.01$ ; GKM: CR = 3.28 g C/m<sup>2</sup>. yr<sup>−2</sup>,  $p < 0.05$ ; CBM: CR = 0.75,  $p > 0.05$ ) with quite a bit of inter-annual fluctuation over the past three decades.

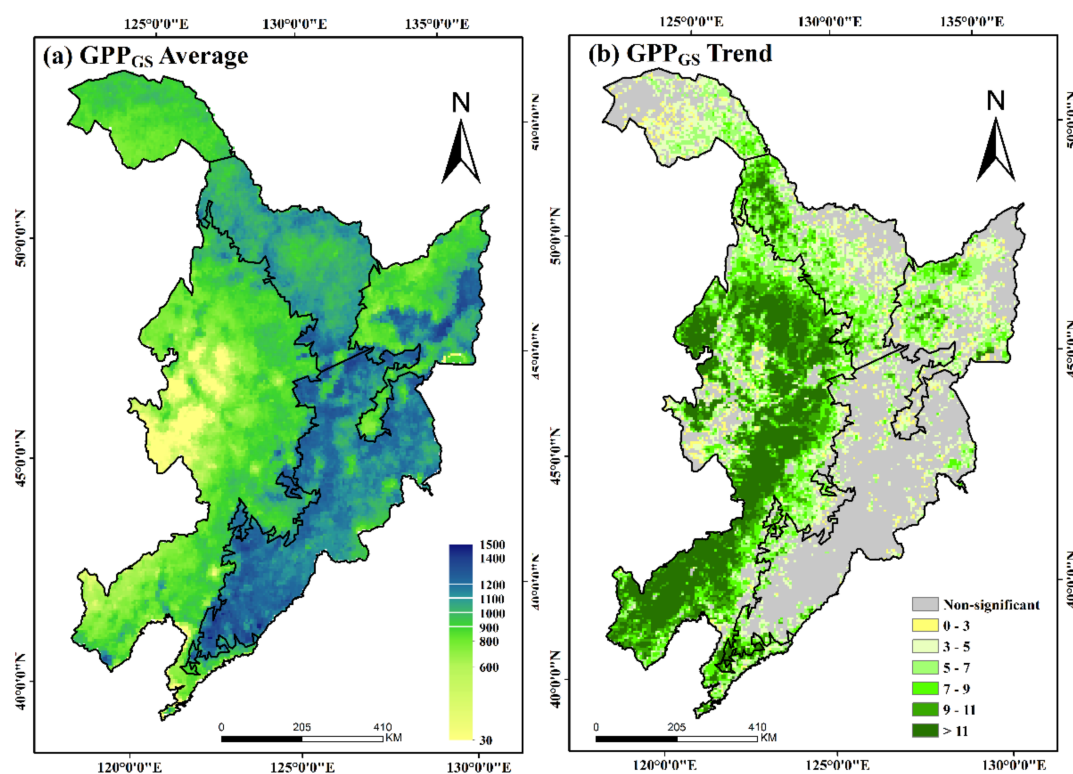


**Figure 2.** Spatial distribution of (a) multi-year average of accumulated gross primary productivity (GPP<sub>GS</sub>) (unit: g C/m<sup>2</sup>·yr<sup>-1</sup>) and (b) inter-annual GPP<sub>GS</sub> trend (unit: g C/m<sup>2</sup>·yr<sup>-2</sup>) across the NEC during 1982–2015.

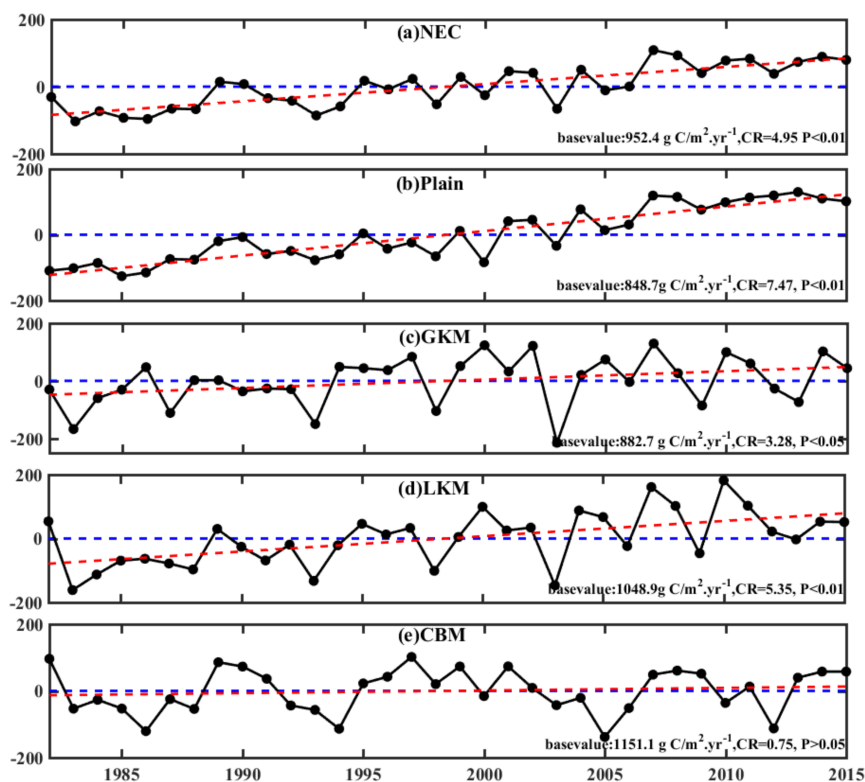


**Figure 3.** Trend of regional GPP<sub>GS</sub> anomalies (true value of GPP<sub>GS</sub> minus multi-average GPP<sub>GS</sub>) from 1982 to 2015 in five zones (the Greater Khingan Mountain (GKM), Lesser Khingan Mountain (LKM), the ChangBai Mountain (CBM), and Plain and the whole NEC) of the NEC (Here, the base value (the blue line) is the multi-year average GPP<sub>GS</sub> from 1982 to 2015; CR refers to the change ratio of GPP<sub>GS</sub> (g C/m<sup>2</sup>·yr<sup>-2</sup>), and P refers to the significance testing. The red line is a trend line calculated by the MK algorithm.).

### 3.2. Relationship between $GPP_{GS}$ and Meteorological Factors

Figure 4 shows a warming, wetting, and dimming trend across the whole NEC, and the impacts of this climate change on vegetation  $GPP_{GS}$  are analyzed in the following sections.

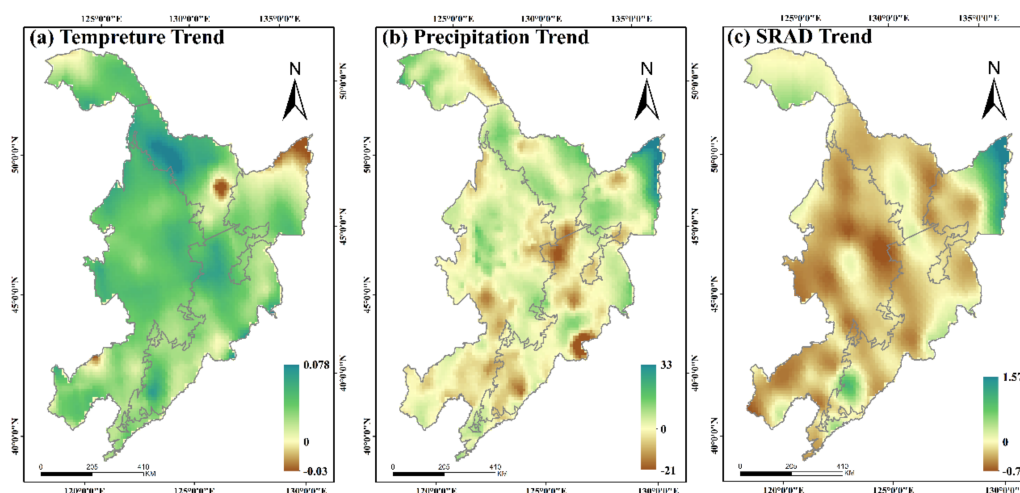


**Figure 4.** The inter-annual trend of (a) yearly average temperature, (b) yearly accumulated precipitation, and (c) yearly average SRAD (Shortwave Radiation) within the growing season across the NEC from 1982 to 2015.

Table 1 indicates that  $GPP_{GS}$  of the NEC is related with the three meteorological factors (daily average temperature, precipitation, and daily solar radiation), especially the obviously warming; nevertheless, this correlation has a great spatial heterogeneity. In plains, warming (Figure 4a) can improve the productivity of crops, while precipitation (Figure 4b) and solar radiation (Figure 4c) do not have significant impacts. In mountainous areas, positive impacts of warming on forest productivity only exist in high-latitude GKM and LKM, and solar radiation comes into positive effect on  $GPP_{GS}$  in GKM and CBM. Precipitation has a negative effect on  $GPP_{GS}$  of forests according to the correlation results, nevertheless, those negative effects were not significant when eliminating the coupling effects between temperature and radiation with precipitation as partial correlation coefficients display. The difference in correlation and partial correlation results manifest that in the NEC, precipitation indirectly impacts vegetation growth by affecting temperature and solar radiation. For example, there is a remarkable dip in  $GPP_{GS}$  time series of the GKM and LKM in 2003 (Figure 3b,c), which is in line with the small amount of radiation caused by extreme large quantities of precipitation in 2003.

**Table 1.** Correlation coefficient (CC) and Partial correlation coefficient (PCC) between regional accumulated GPP ( $GPP_{GS}$ ) and meteorological factors (daily average temperature, precipitation and daily solar radiation) in different regions (Plain, GKM refers to the Greater Khingan Mountain, LKM refers to the Lesser Khingan Mountain, and the CBM refers to the ChangBai Mountain).

	Temperature		Precipitation		Solar Radiation	
	CC	PCC	CC	PCC	CC	PCC
Plain	0.467 **	0.479 **	0.018	−0.149	−0.134	−0.218
GKM	0.501 **	0.512 **	−0.433 **	−0.165	0.776 **	0.695 **
LKM	0.590 **	0.628 **	−0.376 *	−0.202	0.389 *	0.189
CBM	0.238	0.177	−0.483 **	−0.199	0.567 **	0.391 *

\* Significant at the 5% level; \*\* significant at the 1% level.

The contribution of each meteorological factors on  $GPP_{GS}$  can be quantified using the SMLR method, and thus the dominant meteorological factors for  $GPP_{GS}$  variation over the last three decades can be identified as shown in Figure 5. In mountainous areas, the combination of the three meteorological factors has great impacts on forest productivity.



The inset map in Figure 5 shows that 70.5% of the  $GPP_{GS}$  variation in LKM is caused by these three factors among which temperature is the dominant factor. Meteorological factors can explain 61.0% of the variation in  $GPP_{GS}$  of CBM where solar radiation is the dominant factor. In GKM, climate effects accounts for 84.0% of the variation in  $GPP_{GS}$ , and both temperature and solar radiation are equally important for vegetation productivity.

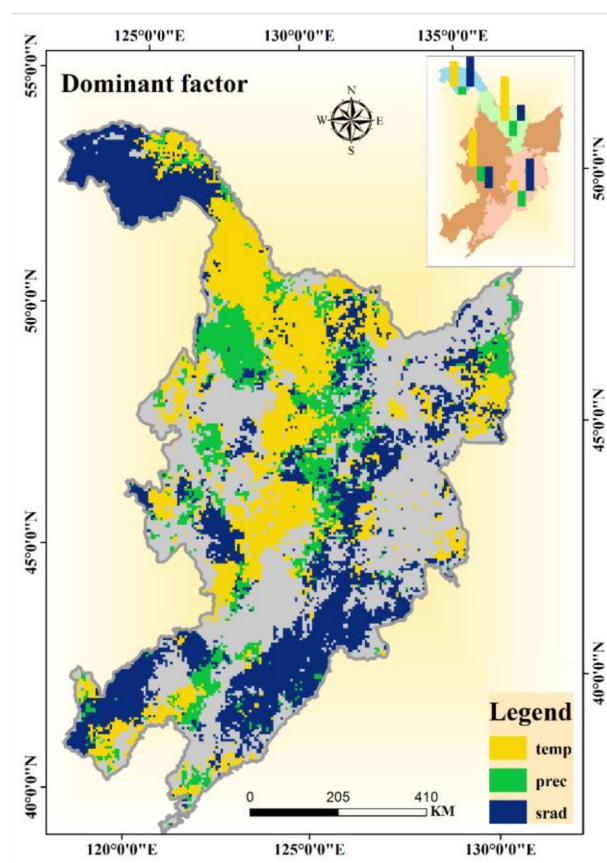


**Figure 5.** Dominant factors for  $GPP_{GS}$  during 1982–2015 at pixel scale (main map) and at regional scale (the inset map).

Contrary to productivity of natural forests in mountainous areas, crops growing in plain are less related with the three meteorological factors, although warming still has positive effect on vegetation productivity in some areas. Furthermore, the linear combination of temperature, precipitation, and solar radiation can only explain 40% of the significant  $GPP_{GS}$  increase in crops, indicating that some other facilitating factors exist for crop productivity increments in the NEC.

### 3.3. Relationship between GPP and LAI

The comparison between GPP and LAI is noteworthy. We download GLASS-LAI products with an 8-day temporal resolution and  $0.05^\circ$  spatial resolution from 1982 to 2015 [39,53,54] and then pre-processed it to a 34-year time series of mean value of LAI within the growing season (denoted as  $LAI_{GS}$ ) across the whole NEC (Figure 6a). The detection of LAI trend across the NEC shows a dramatic increase in  $LAI_{GS}$  across the whole NEC over the last 30 years (Figure 6b). It is the same as the widely reported worldwide greening [8,55–57].

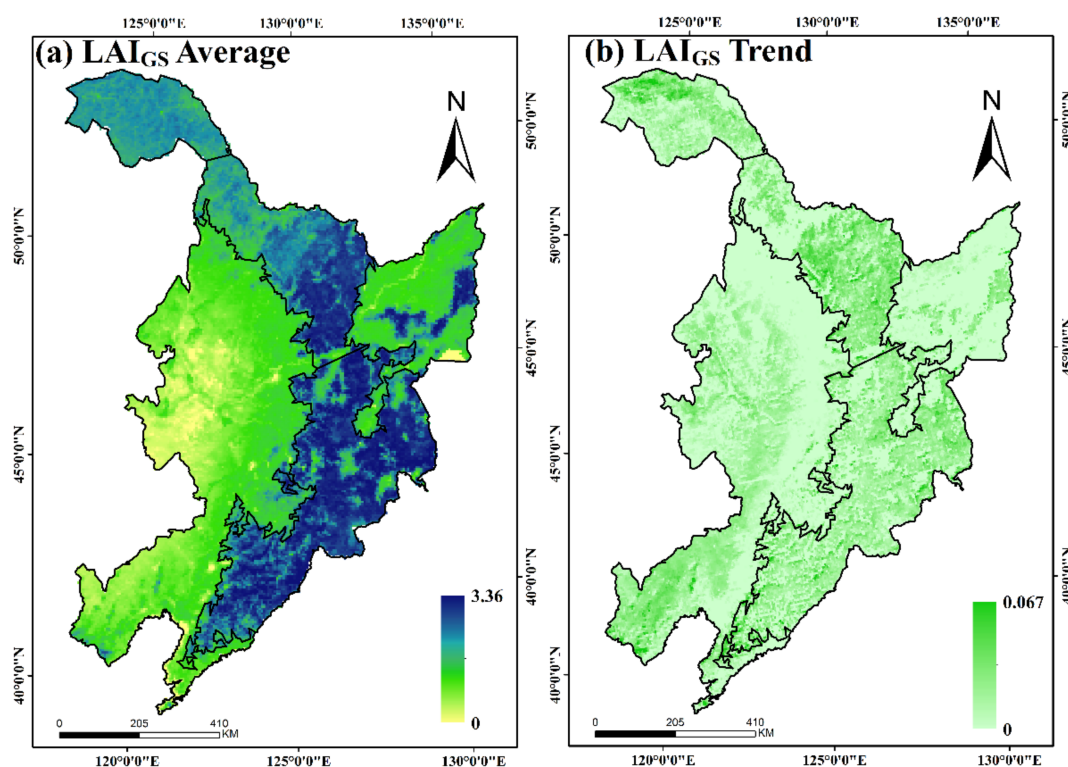


**Figure 6.** Spatial distribution of (a) multi-year average mean value of LAI within the growing season ( $LAI_{GS}$ ) and (b) trend in  $LAI_{GS}$  across the NEC from 1982 to 2015.

Different from the significant increase in  $LAI_{GS}$  across the whole NEC as Figure 6b shows, there is a relatively smaller increment of  $GPP_{GS}$  in forested region across the NEC (the slight increment in the GKM and LKM, and even no increments of  $GPP_{GS}$  in the CBM); quantitatively, the absolute change ratio (ACR) and relative change ratio (RCR, defined as  $\frac{ACR \times \text{study period}}{\text{multi-year mean value}}$ ) of  $GPP_{GS}$  and  $LAI_{GS}$  in each part of the NEC are displayed in Table 2. In forested regions, the increments of  $LAI_{GS}$  are larger than that of  $GPP_{GS}$ , especially in CBM, while, in croplands, the RCR of  $GPP_{GS}$  is twice that of  $LAI_{GS}$ . The relationship between  $GPP_{GS}$  and  $LAI_{GS}$  seems to vary in different regions.

**Table 2.** The absolute change ratio (ACR) and relative change ratio (RCR) of  $GPP_{GS}$  and mean value of LAI within the growing season ( $LAI_{GS}$ ) from 1982 to 2015 across the NEC.

	$GPP_{GS}$		$LAI_{GS}$	
	ACR	RCR	ACR	RCR
GKM	2.88	11.24	0.014	22.26
LKM	4.77	15.51	0.012	17.46
CBM	0.79	2.33	0.012	15.84
Plain	7.345	29.75	0.0057	15.18

According to correlation analysis (Figure 7),  $GPP_{GS}$  is correlated with  $LAI_{GS}$  in relatively high-latitude forests (GKM:  $R = 0.652$ ,  $p < 0.05$ ; LKM:  $R = 0.691$ ,  $p < 0.05$ ) and parts of cropland; however, in mid-latitude CBM, there is non-significant correlation ( $R = 0.334$ ;  $p > 0.05$ ), indicating that GPP is not always changing simultaneously with LAI.

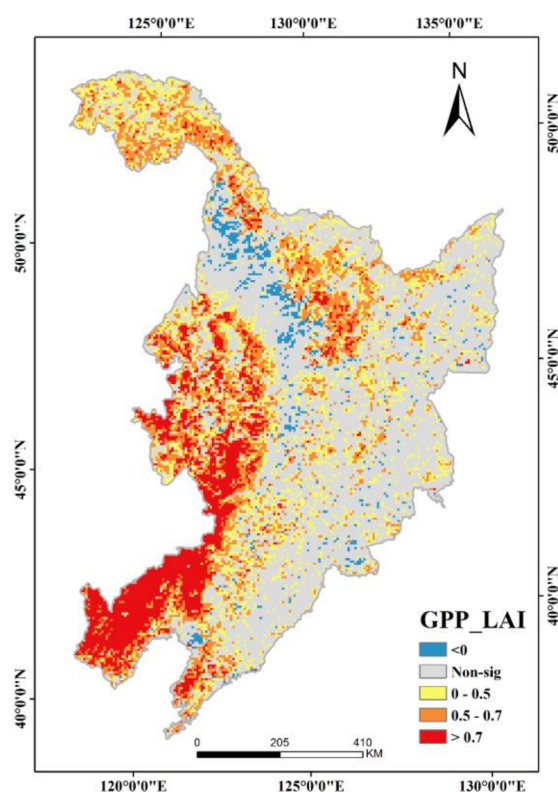


**Figure 7.** Spatial distribution of the correlation coefficient between  $GPP_{GS}$  and  $LAI_{GS}$  across the entire NEC.

## 4. Discussion

### 4.1. Differences of Crops and Forests in $GPP_{GS}$ Trend

In both pixel or regional scales, the inter-annual variation trend of  $GPP_{GS}$  in the NEC (Figures 2 and 3) indicates that the crops growing in plains provide the majority inter-annual increments of terrestrial ecosystem productivity while forests in mountainous area contribute less in productivity increasing over the last 30 years. Furthermore, meteorological factors are not much important for crops in the NEC (Figure 5). Previous studies [58–60] identify two main reasons for the variation of crop productivity, i.e., climate change and agricultural technological progress. Fang et al. (2000) [60] concluded that agricultural technological progress plays a much more important role than climate for rice yield in Heilongjiang, which may be suited for the whole NEC.

The relationship between  $GPP_{GS}$  of crops and the three human intervention indices (IA, CA, and CYA) are displayed in Figure 8. All these indices are highly correlated with  $GPP_{GS}$  where the IA ( $R = 0.897$ ,  $p < 0.05$ ) owns the largest correlation, followed by the CA ( $R = 0.896$ ,  $p < 0.05$ ), and finally, the CYA ( $R = 0.784$ ,  $p < 0.05$ ). The increments of vegetation productivity of crops in the NEC benefits greatly from human intervention (e.g., fertilization, irrigation, and cropland area expansion), instead of meteorological factors identified in Table 1, which is in line with Yuan's findings [61].

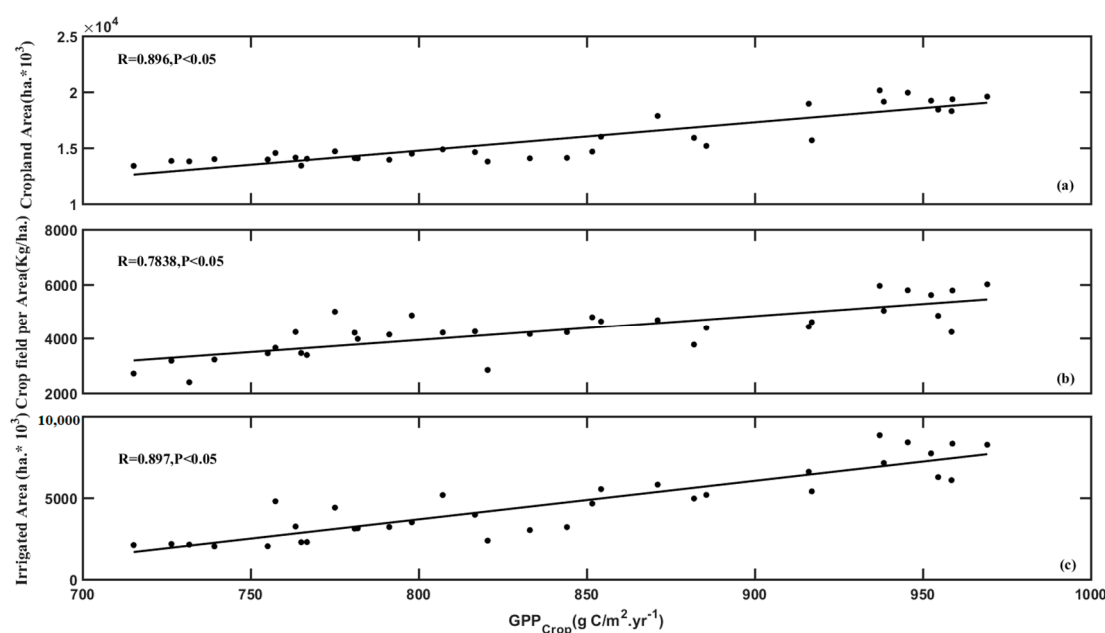


**Figure 8.** Relationship of  $GPP_{GS}$  with (a) Cropland Area, (b) Crop Yield per Area, and (c) Irrigated Area.

All in all, human intervention contributes a lot to vegetation productivity of crops, which greatly facilitates vegetation growth of crops directly leading to the differences of crops and forests in GPP trend.

#### 4.2. Different Trends of GPP and LAI

Song et al. (2017) [62] defined vegetation productivity as a combination of net assimilation rate, LAI, and photosynthesis duration. That is to say, apart from the LAI, net assimilation rate and photosynthesis duration are also decisive for GPP.

Firstly, the net assimilation rate is related with the vegetation type as well as vegetation age. There is a great spatial difference of vegetation type across the whole NEC as Figure 1b and Qian et al.'s study [63] display, so that the relationship between GPP and LAI has great spatial heterogeneity. In addition, the vegetation age is different with time went by which the correlation between GPP and LAI is also influenced. Second, combined with the correlation analysis between GPP and meteorological factors (Figure 5), we found that the CBM is a radiation-dominant region. so, the decreasing trend in solar radiation (or sunshine duration) (Figure 4c) may offset the effect of increasing  $LAI_{GS}$  (Figure 6b), leading to non-significant variation in  $GPP_{GS}$  over the 30 years.

Actually, LAI and GPP describes vegetation growth from two different aspects. LAI is defined as one half of the total green leaf area per unit horizontal ground surface area [64], which aims to quantify the amount of leaf area in an ecosystem [65], so in the NEC, the increasing  $LAI_{GS}$  reflects that the leaf quantity and vegetation coverage of the canopy in the NEC increases, while the small variation in  $GPP_{GS}$  indicates that vegetation's contribution to regional carbon balance has not changed during the three decades of interaction with its environment across the NEC.

In summary, although  $LAI_{GS}$  indicates a greening trend, ecological productivity may not have corresponding variation.  $GPP_{GS}$  may be a more suitable parameter to reflect variation in vegetation growth and vegetation's impacts on carbon cycle [1–7].

#### 4.3. Uncertainties and Future Works

This paper has revealed the slight increasing of  $GPP_{GS}$  in the NEC from 1982 to 2015, and simultaneously identified the effects of climate change on  $GPP_{GS}$ . Nevertheless, some uncertainties still exist for this analysis.



First, we used the GLASS-GPP products which can provide vegetation productivity from 1982; however, the spatial resolution of GLASS-GPP (around 5 km) is rather rough, and thus some variations of GPP may be overlooked, especially in heterogeneous regions, leading to overestimation or underestimation of the trend of vegetation productivity.

Another uncertainty comes from correlation analysis between  $GPP_{GS}$  and three meteorological factors. In this study, we chose the fixed growing season (April to October) of each year as our study period, and then considers the impacts of the three meteorological factors (daily average temperature, precipitation, and daily radiation) within the growing season, nevertheless, these three factors may influence vegetation growth during the whole year. Take temperature as an example, winter temperature also influences spring phenological events of the next year [66]. Therefore, using fixed growing season period as well as considering annual average temperature during growing season to analyze the effects of warming on vegetation productivity may bring some uncertainties. In the next step, we should consider a variable growing season length, such as using temperature thresholds (e.g., 0 and 5 °C) as a sign for growing season, so that a more comprehensive impact of meteorological factors on GPP can be taken into account.

Finally, uncertainty may exist when quantified the effects of each meteorological factors on GPP using SMLR models. The SMLR model assumed that the combined effect of meteorological factors is linear, actually, there is a more complex relationship between  $GPP_{GS}$  and meteorology, in addition, there is a coupling effect between vegetation and atmospheric dynamics, that is to say, apart from the effect brought by climate change on vegetation, the variation of vegetation would impact climate simultaneously as a lot of studies [67–69] have revealed. The relationship between weather and vegetation is too complex to quantify using a statistic-based model. So, a land process models based on biochemical mechanisms, such as CABLE [70], ORCHIDEE [71], and LPJ [72], is needed for more accurate analysis. Apart from reducing uncertainties mentioned above, one important thing that needs further exploration is the relationship between  $GPP_{GS}$  and  $LAI_{GS}$ . This paper found that the relationship between  $GPP_{GS}$  and  $LAI_{GS}$  across the NEC has large spatial heterogeneity, indicating that the widely reported greening is not bound to have great contribution to improve carbon sink capability. Whether this relationship between  $GPP_{GS}$  and  $LAI_{GS}$  found in this paper is specific to the NEC or a common phenomenon in the terrestrial ecosystem is still to be seen.

## 5. Conclusions

This study focuses on the regional feedback of vegetation in the Northeast China (NEC) to the obvious climate change using GLASS GPP products as indicators. Results shows that, from 1982 to 2015,  $GPP_{GS}$  across the NEC has an overall increasing trend ( $4.95 \text{ g C/m}^2 \cdot \text{yr}^{-2}$ ,  $p < 0.01$ ) within which great spatial heterogeneity exists. Vegetation productivity of crops distributing in western NEC is the smallest but has the largest increment ( $7.47 \text{ g C/m}^2 \cdot \text{yr}^{-2}$ ,  $p < 0.01$ ). On the contrary, vegetation productivity of forests is obvious larger than that of crops but only has slight increments in northern NEC (GKM:  $CR = 3.28 \text{ g C/m}^2 \cdot \text{yr}^{-2}$ ,  $p < 0.05$ ; LKM:  $CR = 5.35 \text{ g C/m}^2 \cdot \text{yr}^{-2}$ ,  $p < 0.01$ ) and non-significant variation in southern NEC (CBM).

Correlation analysis between  $GPP_{GS}$  and meteorological factors indicates that warming can improve vegetation productivity of crops as well as forests located in temperature-limited high latitude (GKM and LKM), while this positive effect vanishes in mid-latitude CBM. In addition, for crops of the NEC, apart from the facilitating effect of warming, human intervention plays a decisive role in vegetation productivity increasing over the last 30 years, which directly leads to the difference of crops and forest in  $GPP_{GS}$  trend.

Contrary to the slight or even non-significant variation of vegetation productivity in forested region, an obvious vegetation greening is found across the whole NEC. Correlation analysis between  $GPP_{GS}$  and  $LAI_{GS}$  over the last three decades illustrates that the simultaneously increment of  $GPP_{GS}$  and  $LAI_{GS}$  only exists in high-latitude NEC (GKM and LKM), while in other region, facilitating effect of greening on  $GPP_{GS}$  may be offset by

other factors, such as the shortage of solar radiation in CBM. The different variation trend of GPP<sub>GS</sub> and LAI<sub>GS</sub> reminds us that apart from focusing on vegetation growth dynamics (greening or browning), more attention should be paid on vegetation's feedback to climate as well as its role in carbon cycle.

**Author Contributions:** Conceptualization, L.H. and W.F.; methodology, L.H.; formal analysis, L.H.; writing—original draft preparation, L.H.; writing—review and editing, W.F., W.Y., H.R., and Y.C.; funding acquisition, W.F. All authors have read and agreed to the published version of the manuscript.

**Funding:** This work was supported by the National Natural Science Foundation of China (grant No. 41971301) and the Major Research Development Program of China (2017YFE0122400, 2016YFD0300601).

**Data Availability Statement:** The data presented in this study are available on request from the corresponding author or from the reference website.

**Acknowledgments:** We thank “anonymous” reviewers for their original insights. We are also immensely grateful to the editor for their comments on the manuscript.

**Conflicts of Interest:** The authors declare no conflict of interest.

## References

1. Chapin, M.C.; Matson, P.A.; Mooney, H.A. *Principles of Terrestrial Ecosystem Ecology*, 2nd ed.; Springer: New York, NY, USA, 2002; p. 102.
2. Beer, C.; Reichstein, M.; Tomelleri, E.; Ciais, P.; Jung, M.; Carvalhais, N.; Rödenbeck, C.; Arain, M.A.; Baldocchi, D.; Bonan, G.B.; et al. Terrestrial gross carbon dioxide uptake: Global distribution and covariation with climate. *Science* **2010**, *329*, 834–838. [[CrossRef](#)] [[PubMed](#)]
3. Anav, A.; Friedlingstein, P.; Beer, C.; Ciais, P.; Harper, A.; Jones, C.; Murray-Tortarolo, G.; Papale, D.; Parazoo, N.C.; Peylin, P.; et al. Spatiotemporal patterns of terrestrial gross primary production: A review. *Rev. Geophys.* **2015**, *53*, 785–818. [[CrossRef](#)]
4. Jensen, M.N. Consensus on ecological impacts remains elusive. *Science* **2003**, *299*, 38. [[CrossRef](#)]
5. Cox, P.; Jones, C. Illuminating the modern dance of climate and CO<sub>2</sub>. *Science* **2008**, *321*, 1642–1644. [[CrossRef](#)]
6. Battin, T.J.; Kaplan, L.A.; Findlay, S.; Hopkinson, C.S.; Marti, E.; Packman, A.I.; Newbold, J.D.; Sabater, F. The boundless carbon cycle. *Nat. Geosci.* **2009**, *2*, 598–600. [[CrossRef](#)]
7. IPCC. Land Use, Land-Use Change, and Forestry. In *Cambridge University Press*; Cambridge University Press: Cambridge, UK, 2000; pp. 1–51.
8. Zhu, Z.; Piao, S.L.; Myneni, R.B.; Huang, M.; Zeng, N. Greening of the earth and its drivers. *Nat. Clim. Chang.* **2016**, *6*, 791. [[CrossRef](#)]
9. Chen, C.; Park, T.; Wang, X.; Piao, S.; Xu, B.; Chaturvedi, R.K.; Fuchs, R.; Brovkin, V.; Ciais, P.; Fensholt, R.; et al. China and India lead in greening of the world through land-use management. *Nat. Sustain.* **2019**, *2*, 122–129. [[CrossRef](#)] [[PubMed](#)]
10. Monteith, J.L. Solar radiation and productivity in tropical ecosystems. *J. Appl. Ecol.* **1972**, *9*, 747–766. [[CrossRef](#)]
11. Monteith, J.L. Climate and the efficiency of crop production in Britain. *Phil. Trans. R. Soc. B* **1977**, *281*, 277–294.
12. Martínez, B.; Sanchez-Ruiz, S.; Gilabert, M.A.; Moreno, A.; Campos-Taberner, M.; García-Haro, F.J.; Trigo, I.F.; Aurela, M.; Brümmer, C.; Carrara, A.; et al. Retrieval of daily gross primary production over Europe and Africa from an ensemble of SEVIRI/MSG products. *Int. J. Appl. Earth Obs.* **2018**, *65*, 124–136. [[CrossRef](#)]
13. Running, S.W.; Nemani, R.R.; Heinsch, F.A.; Zhao, M.; Reeves, M.; Hashimoto, H. A continuous satellite-derived measure of global terrestrial primary production. *Bioscience* **2004**, *54*, 547–560. [[CrossRef](#)]
14. Chen, Y.; Gu, H.; Wang, M.; Gu, Q.; Ding, Z.; Ma, M.; Liu, R.; Tang, X. Contrasting Performance of the Remotely-Derived GPP Products over Different Climate Zones across China. *Remote Sens.* **2019**, *11*, 1855. [[CrossRef](#)]
15. Ferreira, R.R.; Mutti, P.; Mendes, K.R.; Campos, S.; Marques, T.V.; Poliveira, C.; Gonçalves, W.; Mota, J.; Difante, G.; Urbano, S.A.; et al. An assessment of the MOD17A2 gross primary production product in the Caatinga biome, Brazil. *Int. J. Remote Sens.* **2021**, *42*, 1275–1291. [[CrossRef](#)]
16. Yuan, W.; Liu, S.; Zhou, G.; Zhou, G.; Tieszen, L.L.; Baldocchi, D.; Bernhofer, C.; Gholz, H.; Goldstein, A.H.; Goulden, M.L.; et al. Deriving a light use efficiency model from eddy covariance flux data for predicting daily gross primary production across biomes. *Agric. For. Meteorol.* **2007**, *143*, 189–207. [[CrossRef](#)]
17. Yuan, W.; Liu, S.; Yu, G.; Bonnefond, J.M.; Chen, J.; Davis, K.; Desai, A.R.; Goldstein, A.H.; Gianelle, D.; Rossi, F.; et al. Global estimates of evapotranspiration and gross primary production based on MODIS and global meteorology data. *Remote Sens. Environ.* **2010**, *114*, 1416–1431. [[CrossRef](#)]
18. Chen, Z. Spatiotemporal variation of productivity and carbon use efficiency of Northeast forests in China from 2000 to 2015. *Chin. J. Appl. Ecol.* **2019**, *30*, 1625–1632.
19. Zhao, J.F.; Yan, X.D.; Jia, G.S. Simulation of carbon stocks of forest ecosystems in Northeast China from 1981 to 2002. *Chin. J. Appl. Ecol.* **2009**, *20*, 241–249.

20. Zhao, X.L. Influence of climate change on agriculture in Northeast China in recent 50 years. *J. Northeast Agric. Univ.* **2010**, *41*, 144–149.
21. Liu, Z.J.; Yang, X.G.; Wang, W.F.; Li, K.N.; Zhang, X.Y. Characteristics of agricultural climate resources in three provinces of Northeast China under global climate change. *Chin. J. Appl. Ecol.* **2009**, *20*, 2199–2206.
22. Ye, D.Z. *Simulation Research on Global Change in China*; China Meteorology Press: Beijing, China, 1992.
23. Guo, L.H.; Wu, S.H.; Zhao, D.S.; Yin, Y.H.; Leng, G.Y.; Zhang, Q.Y. NDVI-based vegetation change in Inner Mongolia from 1982 to 2006 and its relationship to climate at the biome scale. *Adv. Meteorol.* **2014**, 1–12. [[CrossRef](#)]
24. Hou, W.; Gao, J.; Wu, S.; Dai, E. Interannual variations in growing-season NDVI and its correlation with climate variables in the southwestern karst region of China. *Remote Sens.* **2015**, *7*, 11105–11124. [[CrossRef](#)]
25. Wu, C.; Venevsky, S.; Sitch, S.; Yang, Y.; Wang, M.; Wang, L.; Gao, Y. Present-day and future contribution of climate and fires to vegetation composition in the boreal forest of China. *Ecosphere* **2017**, *8*, e01917. [[CrossRef](#)]
26. Zoran, M.A.; Zoran, L.F.V.; Dida, A.I. Forest vegetation dynamics and its response to climate changes. In Proceedings of the Conference on Remote Sensing for Agriculture, Ecosystems, and Hydrology XVIII, Edinburgh, UK, 26–29 September 2016.
27. Yuan, W.P.; Zheng, Y.; Piao, S.L.; Ciais, P.; Lombardozzi, D.; Wang, Y.P. Increased atmospheric vapor pressure deficit reduces global vegetation growth. *Sci. Adv.* **2019**, *5*. [[CrossRef](#)] [[PubMed](#)]
28. Guo, J.T.; Hu, Y.M.; Xiong, Z.P.; Yan, X.L.; Li, C.L.; Bu, R.C. Variations in Growing-Season NDVI and Its Response to Permafrost Degradation in Northeast China. *Sustainability* **2017**, *9*, 551. [[CrossRef](#)]
29. Hu, S.; Liu, J.; Mao, X.G. Extraction and Change of Vegetation Coverage of 2007–2010 in Northeast China. *J. Northeast. For. Univ.* **2017**, *45*, 45–50.
30. Ni, X.L.; Xie, J.F.; Zhou, Y.K.; Gao, X.Z.; Ding, L. Evaluating vegetation growing season changes in northeastern China by using GIMMS LAI3g data. *Climate* **2017**, *5*, 37. [[CrossRef](#)]
31. Zu, J.X.; Yang, J. Temporal variation of vegetation phenology in northeastern china. *Acta Ecol. Sin.* **2016**, *36*, 2015–2023.
32. Yao, J.; He, X.Y.; Li, X.Y.; Chen, W.; Tao, D.L. Monitoring responses of forest to climate variations by Modis NDVI: A case study of Hun river upstream, northeastern china. *Eur. J. Forest Res.* **2012**, *131*, 705–716. [[CrossRef](#)]
33. Tang, H.; Li, Z.; Zhu, Z.; Chen, B.; Zhang, B.; Xin, X. Variability and climate change trend in vegetation phenology of recent decades in the greater khingan mountain area, northeastern china. *Remote Sens.* **2015**, *7*, 11914–11932. [[CrossRef](#)]
34. Liu, D.; Yu, C.L. Estimation on climatic productivity of vegetation NPP in northeastern china based on Modis. *Res. Soil Water Conserv.* **2017**, *24*, 315–323.
35. Liu, X.; Guo, Q.; Wang, C. Simulating net primary production and soil-surface CO<sub>2</sub> flux of temperate forests in Northeastern China. *Scand. J. Forest Res.* **2011**, *26*, 30–39. [[CrossRef](#)]
36. Zhao, J.F.; Yan, X.D.; Guo, J.P.; Jia, G.S. Evaluating spatial-temporal dynamics of net primary productivity of different forest types in northeastern china based on improved FORCCHN. *PLoS ONE* **2012**, *7*. [[CrossRef](#)]
37. Ji, Y.; Zhou, G.; Luo, T.; Dan, Y.; Zhou, L.; Lv, X. Variation of net primary productivity and its drivers in China's forests during 2000–2018. *Forest Ecosyst.* **2020**, *7*, 15. [[CrossRef](#)]
38. EarthData Search. Available online: <https://search.earthdata.nasa.gov/> (accessed on 17 February 2021).
39. Global Land Surface Satellite (GLASS) Products Download and Service. Available online: <http://glass-product.bnu.edu.cn/> (accessed on 17 February 2021).
40. National Center for Atmospheric Research Staff (Ed.) The Climate Data Guide: NASA MERRA. 10 June 2019. Available online: <https://climatedataguide.ucar.edu/climate-data/nasa-merra> (accessed on 17 February 2021).
41. Savitzky, A.; Golay, M. Smoothing and differentiation of data by simplified least squares procedures. *Anal. Chem.* **1964**, *36*, 1627–1638. [[CrossRef](#)]
42. He, J.; Yang, K.; Tang, W.; Lu, H.; Qin, J.; Chen, Y.Y.; Li, X. The first high-resolution meteorological forcing dataset for land process studies over China. *Sci. Data* **2020**, *7*, 25. [[CrossRef](#)]
43. National Tibetan Plateau Third Pole Environment Data Center. Available online: <http://westdc.westgis.ac.cn/data/> (accessed on 17 February 2021).
44. Rodell, M.; Houser, P.R.; Jambor, U.E.A.; Gottschalck, J.; Mitchell, K.; Meng, C.J.; Arsenault, K.; Cosgrove, B.; Radakovich, J.; Bosilovich, M.; et al. The global land data assimilation system. *Bull. Am. Meteorol. Soc.* **2004**, *85*, 381–394. [[CrossRef](#)]
45. Huffman, G.J.; Bolvin, D.T.; Nelkin, E.J.; Wolff, D.B.; Adler, R.F.; Gu, G.; Hong, Y.; Bowman, K.P.; Stocker, E.F. The TRMM Multisatellite Precipitation Analysis (TMPA): Quasi-Global, Multiyear, Combined-Sensor Precipitation Estimates at Fine Scales. *J. Hydrometeorol.* **2007**, *8*, 38–55. [[CrossRef](#)]
46. Pinker, R.T.; Laszlo, I. Modeling surface solar irradiance for satellite applications on a global scale. *J. Appl. Meteorol.* **1992**, *31*, 194–211. [[CrossRef](#)]
47. National Bureau of Statistics. Available online: <http://www.stats.gov.cn/tjsj/> (accessed on 17 February 2021).
48. Mann, H.B. Nonparametric tests against trend. *Econometrica* **1945**, *13*, 245–259. [[CrossRef](#)]
49. Kendall, M.G. *Rank Correlation Methods*; Charles Griffin Company: London, UK, 1975.
50. Patra, J.P.; Mishra, A.; Singh, R.; Raghuvanshi, N.S. Detecting rainfall trends in twentieth century (1871–2006) over Orissa state, India. *Clim. Chang.* **2012**, *111*, 801–817. [[CrossRef](#)]
51. Yue, S.; Pilon, P. A comparison of the power of the t test, Mann–Kendall and bootstrap tests for trend detection. *Hydrol. Sci. J.* **2004**, *49*, 21–37. [[CrossRef](#)]

52. Ay, M.; Kisi, O. Investigation of trend analysis of monthly total precipitation by an innovative method. *Theor. Appl. Climatol.* **2015**, *120*, 617–629. [[CrossRef](#)]
53. Xiao, Z.Q.; Liang, S.L.; Wang, J.D.; Chen, P.; Yin, X.J.; Zhang, L.Q.; Song, J.L. Use of General Regression Neural Networks for Generating the GLASS Leaf Area Index Product from Time-Series MODIS Surface Reflectance. *IEEE Trans. Geosci. Remote Sens.* **2014**, *52*, 209–223. [[CrossRef](#)]
54. Xiao, Z.Q.; Liang, S.L.; Wang, J.D.; Xiang, Y.; Zhao, X.; Song, J.L. Long-time-series global land surface satellite leaf area index product derived from MODIS and AVHRR surface reflectance. *IEEE Trans. Geosci. Remote Sens.* **2016**, *54*, 5301–5318. [[CrossRef](#)]
55. Piao, S.; Yin, G.; Tan, J.; Cheng, L.; Huang, M.; Li, Y.; Liu, R.; Mao, J.; Myneni, R.B.; Peng, S.; et al. Detection and attribution of vegetation greening trend in china over the last 30 years. *Glob. Chang. Biol.* **2015**, *21*, 1601–1609. [[CrossRef](#)]
56. Myneni, R.B.; Keeling, C.; Tucker, C.; Asrar, G.; Nemani, R. Increased plant growth in the northern high latitudes from 1981 to 1991. *Nature* **1997**, *386*, 698–702. [[CrossRef](#)]
57. Nemani, R.R. Climate-driven increases in global terrestrial net primary production from 1982 to 1999. *Science* **2003**, *300*, 1560–1563. [[CrossRef](#)] [[PubMed](#)]
58. Yun, Y.R.; Fang, X.Q.; Wang, Y.; Tao, J.; Qiao, T.F. Main Grain Crops Structural Change and Its Climate Background in Heilongjiang Province during the Past Two Decades. *J. Nat. Resour.* **2005**, *20*, 697–705.
59. Wang, Z.Y.; Song, K.S.; Li, X.Y.; Zhang, B.; Liu, D.W. Effects of Climate Change on Yield of Maize in Maize Zone of Songnen Plain in the Past 40 Years. *J. Arid Land Resour. Environ.* **2007**, *21*, 112–117.
60. Fang, X.Q.; Sheng, J.F. Human adaptation to climate change: A case study of changes in paddy planting area in Heilongjiang Province. *J. Nat. Resour.* **2000**, *15*, 213–217.
61. Yuan, W.; Liu, S.; Liu, W.; Zhao, S.; Dong, W.; Tao, F.; Chen, M.; Lin, H. Opportunistic market-driven regional shifts of cropping practices reduce food production capacity of China. *Earths Future* **2018**, *6*, 634–642. [[CrossRef](#)]
62. Song, Y.C. *Vegetation Ecology*, 2nd ed.; Higher Education Press: Beijing, China, 2017.
63. Qian, H.; Yuan, X.Y.; Chou, Y.L. Forest Vegetation of Northeast China. In *Forest Vegetation of Northeast Asia*; Kolbek, J., Srutek, M., Box, O.E., Eds.; Springer: Amsterdam, The Netherlands; Berlin/Heidelberg, Germany, 2003; Chapter 6; pp. 181–230.
64. Chen, J.M.; Black, T.A. Defining leaf area index for non-flat leaves. *Plant Cell Environ.* **1992**, *15*, 421–429. [[CrossRef](#)]
65. Fang, H.; Baret, F.; Plummer, S.; Schaepman-Strub, G. An overview of global leaf area index (LAI): Methods, products, validation, and applications. *Rev. Geophys.* **2019**, *57*, 739–799. [[CrossRef](#)]
66. Wang, H.J.; Wu, C.Y.; Ciais, P.; Penuelas, J.; Dai, J.H.; Fu, Y.S.; Ge, Q. Overestimation of the effect of climatic warming on spring phenology due to misrepresentation of chilling. *Nat. Commun.* **2020**, *11*, 4945. [[CrossRef](#)]
67. Chen, C.J.; Chen, C.C.; Lo, M.H.; Juang, J.Y.; Chang, C.M. Central Taiwan's hydroclimate in response to land use/cover change. *Env. Res. Lett.* **2020**, *15*, 034015. [[CrossRef](#)]
68. He, Y.Q.; Lee, E.; Mankin, J.S. Seasonal tropospheric cooling in Northeast China associated with cropland expansion. *Environ. Res. Lett.* **2020**, *15*, 034032. [[CrossRef](#)]
69. Pielke, R.A.; Mahmood, R.; McAlpine, C. Land's complex role in climate change. *Phys. Today* **2016**, *69*, 40. [[CrossRef](#)]
70. Wang, Y.P.; Law, R.M.; Pak, B. A global model of carbon, nitrogen and phosphorus cycles for the terrestrial biosphere. *Biogeosciences* **2010**, *7*, 2261–2282. [[CrossRef](#)]
71. Krinner, G.; Viovy, N.; de Noblet-Ducoudré, N.; Ogée, J.; Polcher, J.; Friedlingstein, P.; Ciais, P.; Sitch, S.; Prentice, I.C. A dynamic global vegetation model for studies of the coupled atmosphere biosphere system. *Glob. Biogeochem. Cycles* **2005**, *19*, GB1015. [[CrossRef](#)]
72. Sitch, S.; Smith, B.; Prentice, I.C.; Arneth, A.; Bondeau, A.; Cramer, W.; Kaplan, J.O.; Levis, S.; Lucht, W.; Sykes, M.T.; et al. Evaluation of ecosystem dynamics, plant geography and terrestrial carbon cycling in the LPJ dynamic global vegetation model. *Glob. Chang. Biol.* **2003**, *9*, 161–185. [[CrossRef](#)]